Electron-Induced Origins of Prebiotic Building Blocks of Sugars: Mechanism of Self-Reactions of a Methanol Anion Dimer

Journal:	*Physical Chemistry Chemical Physics*
Manuscript ID	CP-ART-01-2018-000148.R2
Article Type:	Paper
Date Submitted by the Author:	17-Apr-2018
Complete List of Authors:	Karsili, Tolga; Temple University, Chemistry Fennimore, Mark; Temple University, Department of Chemistry Matsika, Spiridoula; Temple University, Department of Chemistry

Journal Name

ARTICLE TYPE

Cite this: DOI: 10.1039/xxxxxxxxxx

Electron-Induced Origins of Prebiotic Building Blocks of Sugars: Mechanism of Self-Reactions of a Methanol Anion Dimer†

Tolga N. V. Karsili,*[a] Mark A. Fennimore,[a] and Spiridoula Matsika*[a]

Received Date
Accepted Date

DOI: 10.1039/xxxxxxxxxx

www.rsc.org/journalname

The elementary synthesis of prebiotic molecules has attracted vast attention in recent years. Due to their rich surface chemistry and lack of suitable atmosphere, comets represent an important host for such synthesis, especially since they are routinely irradiated with short wavelength electromagnetic radiation and energetic cosmological electrons. Using high-level electronic structure theory, we present the details of the reactivity associated with the electron-impact induced prebiotic synthesis of ethylene glycol (a carbohydrate building block) from elementary methanol. The results suggest that the experimentally observed intermediates and fragment products can be viably formed by both neutral excited-state chemistry and by dissociative electron attachment - highlighting the importance of a theoretical mapping of the relevant potential energy surfaces that ultimately act as an important guide to the experimental results.

1 Introduction

Formation of prebiotic molecules in extraterrestrial environments has been studied both experimentally and theoretically, demonstrating the synthesis of organic molecules, including molecules important for biology such as amino acids, quinones, and nucleobases.[1–3] Methanol ice crystals, as well as other prebiotic building blocks, are ubiquitous in a myriad of interstellar fragments such as comets.[4–6] Such entities do not have a protective layer and are thus routinely irradiated with mid/deep-UV radiation.[5,7,8] These radiative conditions are also known to produce a high yield of secondary electrons - formed by ionization of atomic and molecular fragments present in the interstellar medium (ISM). Recent gas-phase experiments have noted that electron-irradiation (at energies > 6.5 eV) of a beam of jet-cooled methanol leads to C-H and O-H bond fission.[9] The inherent low entropy in a solid-state methanol ice crystal may encourage the recombination of nascent fragments to form long chain sugars (including polysaccharides). The detection of derivatives of methanol, such as ethylene glycol ($HOCH_2CH_2OH$) and methoxymethanol (CH_3OCH_2OH), in ISM supports this idea.[10,11] The nascent sugars formed in the ISM may have reached a prebiotic earth via terrestrial fragment impact - driving a link between elementary molecular fragmentation and an early planetary formation of prebiotic sugar precursors to saccharides. Theoretical studies have outlined the plausible photostability of simple sugars such as glucose and ribose.[12] Both sugars are stable under deep-UV irradiation, suggesting that they may survive the flight-times associated with extraterrestrial fragments. In support of the extraterrestrial formation several sugar related compounds have been found in carbonaceous meteorites like Murchison.[13]

When an electron is incident upon a molecule, an electron scattering or attachment event may occur. A scattering event occurs when an electron-molecule collision leads to deflection of the electron - typically leaving behind an electronically excited neutral molecule. The nascent excited-state may then fragment to form neutral molecular fragments. In contrast, an attachment event occurs when an electron-molecule collision leads to attachment of the incident electron - forming an electron attached state of the molecular anion. The nascent anion is usually highly energetic and leads to molecular fragmentation, forming two or more co-fragments. This is the premise behind dissociative electron attachment (DEA) and has formed the basis of many experimental and theoretical studies.[9,14–17] Despite high interest in DEA processes, extrapolation to the formations of prebiotic biomolecules has received surprisingly little attention despite some recent experiments hinting at their importance.[5,18–21] In the specific case of methanol, studies have highlighted its plausible involvement for forming precursors for prebiotic sugars upon electron-irradiation.[18–20] The neutral absorption spectrum of gas-phase methanol reveals a deep-UV onset (ca. 195 nm) for excita-

[a] Department of Chemistry, Temple University, Philadelphia, PA 19122, USA. Fax: +1 215-204-1532; Tel: +1 215-204-7703; E-mail: smatsika@temple.edu, tolga.karsili@temple.edu

† Electronic Supplementary Information (ESI) available: Information about the orbital stabilization method, natural transition orbitals of excited states, additional potential energy surfaces, and cartesian coordinates of important geometries. See DOI: 10.1039/b000000x/

tion to a $n\sigma^*$ state, which when excited, mediates the formation of a subset of translationally fast fragments.[22] Upon electronic excitation, H-atom elimination is predominantly formed via the classic O-H bond fission channel, forming CH_3O + H fragments, but is also known to be formed *via* a minor C-H bond fission channel - forming CH_2OH + H fragments.[23] In electron-irradiation studies, an analogous O-H bond-fission channel has also been observed (leading to a neutral and an anion fragment).[9] In this case, the incident electron is carried through into the fragment products as H^- - highlighting DEA as the fragmentation mechanism rather than simple scattering of the incident electron. Such electron-induced reactions have also been reported in condensed-phase methanol thin-films, wherein the nascent fragments were proposed to form *via* an intermediate neutral excited state formed by incident electron scattering rather than electron-attachment.[19] This is in contrast to the electron-irradiation studies by Slaughter *et al.* who clearly identify DEA as their dominant reactive process.[9] Although informative, the electron-induced non-DEA mediated fragmentation process claimed in condensed phase studies does not unambiguously rule out an initial preparation of an electron-attached state. In liquid media, the nascent electron-attached state is likely quenched by collisional deactivation followed by vibrational-relaxation - precluding DEA.

In this contribution, we therefore computationally explore the competition between DEA and electron-scattering, and the extent to which each process contributes to the fragmentation dynamics of gas-phase methanol following electron-irradiation. Using high-level electronic-structure theory, the work presented here describes the mechanism associated with the formation of a model sugar precursor ethylene glycol (1,2-dihydroxyethane, henceforth denoted as 1,2-DHE) via the dissociative recombination of a methanol dimer (henceforth $(CH_3OH)_2$):

$$2CH_3OH \rightarrow C_2H_6O_2 + H_2$$

The formation of ethylene glycol has been observed in recent experiments where methanol thin films are irradiated by low energy electrons,[18,19] motivating our choice for this reaction as our model system. It should be noted that other products have been detected from the reaction of two methanols, and future studies can potentially explore the formation of these other products and competition of the various pathways. Furthermore, even though the present study is in the gas phase, we expect that the results will still be very informative and can serve to as a first step in exploration of reactivity in methanol ices.

2 Methodology

2.1 Ground State

The ground state minimum energy geometries of methanol and methanol dimer were optimized using Density Functional Theory (DFT) with the ωB97XD functional[24] and the cc-pVDZ basis set.[25] A relaxed scan along the COOC dihedral angle of the dimer was computed at the same level of theory. ωB97XD/cc-pVDZ was also used to compute the transition state connecting the reactant dimer to the 1,2-DHE + H_2 products, derived using the Synchronous Transit-Guided Quasi-Newton method.[26] The minimum energy path (MEP) along this profile was computed by means of an intrinsic reaction path again using the aforementioned level of theory.

2.2 Neutral Excited and Anionic States

In order to explore the reactivity of excited and anionic states we utilized both single- and multi-reference methods. The Equation of Motion Coupled Cluster with Singles and Doubles (EOM-CCSD) method was used to obtain accurate energetics especially in the Franck-Condon region, with the EOM-EE-CCSD used for excited states while the EOM-EA-CCSD was used for the anionic states.[27] The Complete Active Space second order Perturbation Theory (CASPT2)[28] was used to explore regions beyond the Franck-Condon region and particularly dissociative paths. In describing the neutral states, CASPT2 represents the gold-standard in computing many electronic states that show multi-reference character particularly along dissociative coordinates. It is also essential to describe Feshbach resonances. Details of how these methods are applied in the specific cases studied are outlined below.

2.2.1 Neutral excited states

The excited states of methanol were computed at both the EOM-EE-CCSD and the CASPT2 levels. The EOM-EE-CCSD calculations were performed using the aug-cc-pVDZ basis set while the CASPT2 calculations used cc-pVDZ since a qualitative description along the dissociation path was the primary objective. Unrelaxed, rigid-body potential energy (PE) profiles of methanol were computed along a CH stretching coordinate, using CASPT2 with an active space of (10,8) and a CASSCF averaged over 3 singlet neutral states, 3 triplet neutral states and 5 doublet states of the anion.

The ground and excited neutral states of the methanol dimer, along the MEP computed above, were also computed using both EOM-EE-CCSD and CASPT2 methods. The CASPT2 computations were based on a four state-averaged CASSCF (SA4-CASSCF) with an active space of 14 electrons in 10 orbitals (14,10) coupled to the cc-pVDZ basis set. An imaginary level shift of 0.5 a.u. was used in order to aid convergence and to mitigate the involvement of intruder states. The EOM-EE-CCSD/aug-cc-pVDZ level of theory was also used to compute the neutral ground and excited states along the MEP described above.

2.2.2 Anionic states

EOM-EA-CCSD with the aug-cc-pVDZ and an extra set of even tempered diffuse functions (1s,1p,1d) were used for the anion resonances for the methanol monomer. The orbital stabilization method was used in order to obtain the resonance positions and widths. Analytic continuation combined with the Generalized Padé Approximation (GPA) was used to obtain the widths from the avoided crossings between the resonance states and discretized approximations to the continuum.[29–33] Details of how we apply this approach can be found in ESI† and in our previous publications.[17,34,35]

Ground and excited anion states of the methanol dimer were calculated using EOM-CCSD for electron attachment (EOM-EA-

CCSD) and CASPT2. Here we have used a small basis set (cc-pVDZ) in order to mitigate the involvement of continuum states whilst maintaining a qualitative description (rather than a fully accurate quantitative account) of the topography associated with the reaction herein. We were not able to successfully apply the orbital stabilization method to obtain widths of the resonances for the dimer, but we do not expect the widths to change significantly when compared to the monomer. A caveat here is that our small basis set gives rise to an expected over-estimation of the electron-affinities reported experimentally.[9] That said we have shown in previous studies that the expected over-estimation is consistent across the anion electronic states and that the qualitative topography of the reaction remains unchanged upon increasing basis set size.[17] The CASPT2 computations were based on a 10 state average CASSCF (SA10-CASSCF) reference wavefunction built upon an active space comprising five electrons in eight orbitals (5,8). This small active space was necessary in order to produce smooth curves along the full reaction path. A small imaginary level shift of 0.3 a.u. was used.

In addition to the energies, nonadiabatic derivative couplings between all pairs of anionic states were calculated at the SA9-CASSCF(5,8) level in order to provide more information about nonadiabatic transitions between these states.

All ground state optimizations were undertaken in Gaussian 09[36] whilst all CASPT2 computations were undertaken in Molpro 2010.1.[37] The QChem software was used for the EOM-EE-CCSD and EOM-EA-CCSD calculations.[38] Nonadiabatic couplings were calculated using GAMESS.[39]

3 Results and Discussion

3.1 Methanol Monomer

In order to understand the mechanism associated with the formation of the model sugar precursor, ethylene glycol, we start by considering isolated methanol. Indeed, the work presented herein is motivated by the neutral and anion excited-state energetics of isolated methanol; which has formed the basis of past photodissociation and DEA studies.[9,22,23,40,41]

Table 1 shows the theoretical and experimental excitation energies of isolated methanol. Methanol has three singlet excited states in the energy range between 6.7 and 8.5 eV. These states represent excitations to Rydberg states that are characterized by ($2a''\rightarrow$ 3s) and ($2a'' \rightarrow$ 3p) electron promotions. The natural transition orbitals, associated with the aformentioned excitations are given in ESI† (Fig. S2). The weak oscillator strength (0.004) associated with the S_1-S_0 excitation (at $\approx$ 6.7 eV) is characteristic of the poor spatial overlap between the orthogonal 2a$''$ and 3s orbitals. In contrast, excitation to the subsequent two electronic states (i.e. the S_2-S_0 and S_3-S_0 transitions) contain an order of magnitude stronger oscillator strength when compared with the S_1-S_0 transition. There are also two triplet states in this energy range with the lowest one, T_1, about 0.3 eV below the lowest singlet state. Comparisons with the experiments, obtained from either UV absorption spectroscopy[42] or via low energy electron impact,[43] show that the EOM-EE-CCSD/aug-cc-pVDZ results reproduce the experimental values within 0.1 eV except for T_2. Whilst the CASPT2 energies overestimate the experimentally measured values, they provide a qualitative description of the states, and these calculations are most useful along dissociation paths and when multireference effects become important (*vide infra*).

Table 1 Excited state energies in eV and oscillator strengths in parenthesis of methanol calculated in this work and compared with experimental values obtained either from absorption cross sections[42] or via low energy electron impact.[43]

	EOM-EE-CCSD	CASPT2	exp[43]	exp[42]
T_1	6.58	7.29	6.40	
S_1	6.73 (0.004)	7.76	6.70	6.76(0.0051)
T_2	7.95	8.87	7.47	
S_2	7.91 (0.038)	9.47	7.83	7.73(0.034)
S_3	8.49 (0.042)			8.31(0.041)

In addition to the neutral electronic states we also examined the resonances of the methanol monomer, which play a pivotal role in electron driven chemistry. Table 2 lists the theoretically derived and experimentally measured energetic positions and widths of the various resonances of the methanol monomer. In the present work, resonances were computed at the EOM-EA-CCSD/aug-cc-pVDZ+1s,1p,1d level, using orbital stabilization methods as outlined in Section 2. To the best of our knowledge only a single study has identified the energetic position of a shape resonance at $\approx$ 3 eV.[44]. In contrast, there is a wealth of data associated with the long-lived Feshbach resonances, which have been identified at energies $\geq$ 6.5 eV, and are known to be important in electron driven chemistry. Our computations identify the lowest Feshbach resonance at 6.63 eV, which is in very good agreement with previously obtained experimental and theoretical results (see Table 2). The presently derived lifetime is however more than an order of magnitude shorter than previous theoretical values, but we recognize that the widths are expected to contain a larger theoretical error when compared with the energetic positions. Notwithstanding, scattering theory predicts a sufficiently long lifetime (of several picoseconds) for this Feshbach resonance.

Table 2 Positions (and widths in parenthesis) of resonances of methanol given in eV calculated using EOM-EA-CCSD. Widths from Ref.[45] are also converted to lifetimes. $^{\alpha}$Correspond to shape resonances, while all the others are Feshbach resonances.

this work	exp[46]	exp[47]	theory[45]	Lifetime/fs[45]
1.67 (0.94)$^{\alpha}$	3[44]$^{\alpha}$			
6.63 (0.07)	6.4	6.5	6.75 (0.001)	4100
	7.9	8	8.81 (0.0027)	1500
	10.2	10.5	11.73 (0.0567)	73

In order to better understand the proposed mechanism and important electronic states for forming ethylene glycol *via* H_2 elimination in the ensuing manuscript, we have examined the way in which the various neutral and anionic states of methanol vary as a function of C-H bond elongation. Fig. 1 presents the PE profiles for isolated methanol, along the C-H bond extension coordinate. The black and grey curves represent, respectively, the singlet and triplet states of the neutral molecule, whilst the red curves represent the anion doublet states. In the neutral molecule, Fig. 1

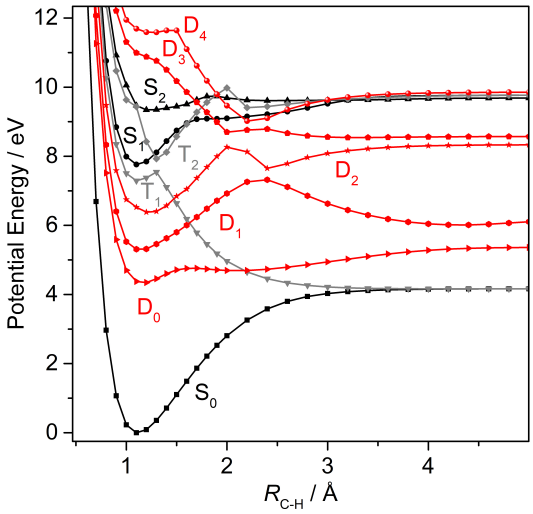

Fig. 1 CASPT2/cc-pVDZ potential energy profiles of isolated methanol, along the C-H bond extension coordinate.

shows that the only dissociative curve, which ultimately correlates with the ground state asymptotic products is T_1. Such an effect can be traced back to the photodissociation of methane and may be understood by considering the long-range repulsive interaction between a pair of parallel-spin pσ-electrons. Attachment of an electron to the lower energy orbital of the T_1 state electronic configuration leads to the D_0 shape resonance. The D_0 state represents an odd electron occupancy in a σ^* virtual orbital and is thus dissociative with respect to C-H bond elongation, forming the ground state CH_2OH + H asymptotic products. This dissociative nature is not optimally captured in Fig. 1 due to the required use of a small basis set (see methodology for reasoning) and a lack of optimization of the equilibrium geometry as a function of C-H stretch. In contrast, electron-attachment to the higher energy orbital of the T_1 configuration represents a core-excited Feshbach resonance and can be vertically identified as D_3. Diabatically, the myriad of avoided crossings indicate that the electronic state character of D_3 becomes D_2 and then finally, D_1 upon progressive C-H bond elongation - representing a dissociative C-H stretch dependence that correlates with the first electronically excited CH_2OH + H asymptotic products. Extrapolating this logic to the methanol dimer will yield analogous electronic states that are reactive with respect to C-H bond stretch, with the additional caveat that the nascent radicals may self-react to form longer-changed hydrocarbons. We explore this possibility in the remainder of this manuscript.

3.2 Methanol Dimer

3.2.1 Ground-state structures

As shown in the introduction, the formation of ethylene glycol in our model system requires the elimination of molecular H_2 following a self-reaction between a pair of methanol molecules. It is therefore intuitive to start the discussion by considering the ground state reactivity associated with the elimination of H_2 from $(CH_3OH)_2$. Fig. 2 displays the ground state optimized geometry of $(CH_3OH)_2$. As expected, OH–OH hydrogen-bonding dominates the intermolecular interactions, giving a global minimum energy geometry which is analogous to that observed in small water-clusters.[48,49] Within this configuration, the individual methanol molecules exist in a staggered conformation in order to reduce the steric hindrance encountered by the methyl moieties. Rotation about the OH–O hydrogen-bond therefore represents a Newman-projection. Fig. 3 presents the PE profile as a function of rotation about the OH–O hydrogen-bond. The PE profile is analogous to that observed upon rotation about C-C bonds in aliphatic hydrocarbons - in which maxima and minima along the profile respectively represent the eclipsed and staggered conformations of the bulking substitutes attached to each of the two C atoms that make up the C-C bond. In much the same way, the return maxima and minima in Fig. 3 represent, respectively, the eclipsed and staggered conformations of the methyl moieties. It is important to note that the maxima are qualitatively much lower than in analogous hydrocarbons (e.g. butane). This can be understood by considering the much longer OH–O bonding distance when compared to a typical C-C bond distance in an aliphatic hydrocarbon - i.e. that the steric hindrance experienced by the methyl groups, even at an eclipsed conformation, is much smaller in $(CH_3OH)_2$ (cf. butane). The energy at the maxima in Fig. 3 is comparable to room-temperature thermal energy (3/2)kT, but we note that within the low temperature regime of the ISM, such conformational changes may become important. We therefore use the staggered global minimum energy geometry (as displayed in Fig. 2) as the starting geometry for the ensuing reactivity.

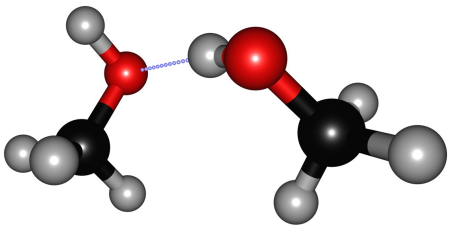

Fig. 2 The ground state minimum energy geometry of $(CH_3OH)_2$

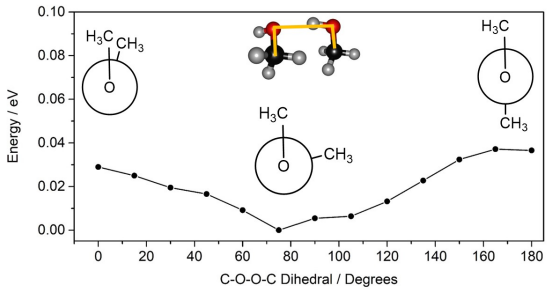

Fig. 3 Relaxed potential energy profiles (and accompanying Newman-projections) associated with rotation about the C-O-O-C dihedral angle - The yellow highlight indicates the dihedral angle.

Table 3 Excited states in eV and oscillator strengths in parenthesis of methanol dimer calculated at the minimum using EOM-EE-CCSD/aug-cc-pVDZ and CASPT2/cc-pVDZ

	EOM-EE-CCSD	CASPT2
T_1	6.92	
S_1	6.96 (0.0004)	7.97
S_2	7.02 (0.0047)	8.10
S_3	7.56 (0.0375)	9.51
S_4	7.80 (0.0095)	

3.2.2 Neutral reaction paths

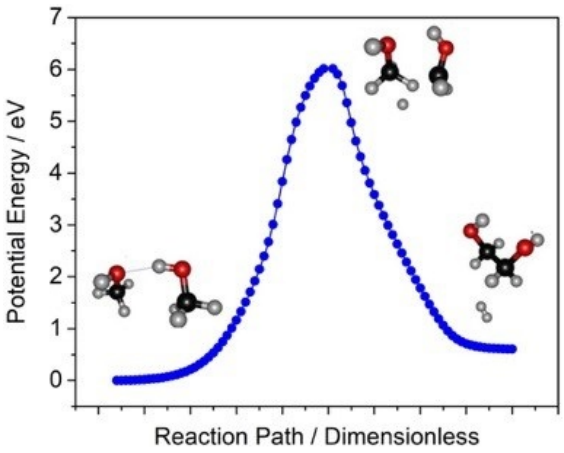

Fig. 4 Minimum energy path connecting methanol dimer reactant to the ethylene glycol + H_2 products via the optimized transition state calculated using DFT.

In order to describe the reaction of methanol dimer, we first located a transition state (TS) connecting the global minimum energy geometry to that of 1,2-DHE + H_2 products using DFT (see methodology for details). As the TS geometry in Fig. 4 illustrates, both methanol molecules, that make up the dimer, contain an elongated C-H bond - indicating C-H bond fission. The departing H atoms show an optimal alignment for forming H_2. Using the optimized TS, a minimum energy path (MEP) connecting $(CH_3OH)_2$ to the 1,2-DHE + H_2 products was obtained. The calculated MEP is displayed in Fig. 4 and shows that the $(CH_3OH)_2$ $\rightarrow$ 1,2-DHE + H_2 reaction in the electronic ground state is hindered by an energetic barrier of $\approx$ 6 eV. This restrictive barrier precludes a viable reaction on the electronic ground state.

We therefore turn our attention to the electronically excited states associated with this reaction. The excitation energies of the dimer at the equilibrium geometry are shown in Table 3. The EOM-EE-CCSD energies show that the analogous monomer states are split into two distinct states - highlighting excitation localized on one or both methanol moities that make up the dimer. The natural transition orbitals describing the excited states are shown in ESI† (Fig. S3). The brightest state is now S_3, which is predicted at 7.6 eV. The lowest triplet state has very similar energy to the lowest singlet state, with a negligible gap between them. The energies derived by EOM-EE-CCSD were then compared to CASPT2/cc-pVDZ. The results show that whilst the excitation energies derived with the latter are in good agreement with EOM-EE-CCSD, those derived from the former overestimate the EOM-EE-CCSD energies by $\approx$ 1 eV.

In order to examine the reactivity of the excited states, these were calculated along the MEP obtained from the ground state focusing on the reactive side between reactants and transition state. Even though this is not the optimum way to examine the reactivity of the excited states it provides important information about how the energies change along this path. Fig. 5 shows the excited-state energies along the path connecting the reactants to the TS, computed at the EOM-EE-CCSD/aug-cc-pVDZ level. In order to ensure that this method captures the correct behavior of excited states the calculations were also performed at the CASPT2/cc-pVDZ level (shown in ESI†, Fig. S5). The excited states behave qualitatively very similarly with both methods, but EOM-EE-CCSD gives more accurate quantitative energetics. As shown in Fig. 5, the ground state largely mimics the MEP profile displayed in Fig. 4. The initial part (R(C-C) $\geq$ 2.5 Å) of the S_1, S_2, S_3 and S_4 states shows a net rise in PE along the reaction path - indicating a lack of driving force for reaction near the Franck-Condon region. Despite this initial unreactivity, the gradients associated with the S_1, S_2 and S_3 states are somewhat shallower than that for S_0; indeed, upon decreasing R(C-C) (R(C-C) $<$ 2.5 Å) the profile of the S_1 state becomes reactive - driving the possibility for S_1 to S_0 internal conversion (IC) near the transition state. If the excited state is prepared by electron scattering the triplet state can also be generated. The lowest triplet state is shown in Fig. 5 as well. This state initially has almost the same energy as S_1 but as it approached the transition state it gets more stabilized and at the TS a crossing with the ground state is shown. The overall behavior suggests that this state may be more reactive than the singlet manifold. Overall a neutral pathway requires an excitation in the deep-UV ($>$ 7 eV). That said, such states may be populated in ISM either via energetic electrons or deep-UV/near-X-ray irradiation.

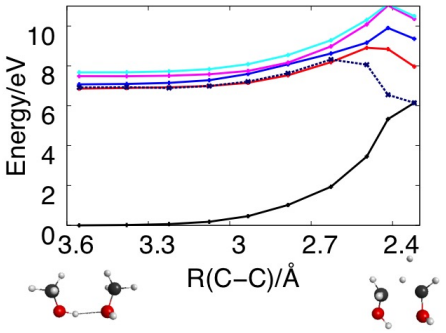

Fig. 5 Potential energy profiles associated with the ground and electronically excited states of neutral dimer along the minimum energy profile calculated using EOM-EE-CCSD/aug-cc-pVDZ. Singlet states are shown with solid lines and triplet with dashed lines.

3.2.3 Anion reaction paths

We now turn our attention to the ways in which the PE profiles associated with the anion states of $(CH_3OH)_2$ vary along the reaction path and how these compare with the neutral electronic

states.

Fig. 6 presents PE profiles of the lowest nine doublet states as a function of R(C-C) of the −1 anion - calculated using CASPT2/cc-pVDZ. The black curves represent the shape resonances whilst the red curves represent the core-excited Feshbach resonances. Describing the higher ionic states on the product side is difficult with CASPT2 and as these states are not relevant only the lowest two relevant states are shown on the product side. Analogous profiles, computed at the EOM-EA-CCSD/cc-pVDZ level of theory, are presented in ESI† (Fig. S6) and the lowest shape resonances are qualitatively similar to those displayed in Fig. 6, but it is much more difficult to obtain Feshbach resonances. Since these are crucial here we rely on the CASPT2 methods for the profile.

In the dimer both shape and Feshbach resonances are energetically similar to those derived in the methanol monomer. Though energetically accessible, the lowest shape resonances have very short lifetimes and are therefore expected to be limited by electron-detachment and unlikely to promote electron driven chemistry. On the other hand, the lifetimes of the Feshbach resonances are expected to be much longer (by analogy to the several picosecond lifetime reported for the methanol monomer). As such, electron-driven chemistry is likely to out-compete electron detachment given the ultrafast nuclear dynamics expected from the high density of states present in the anion.

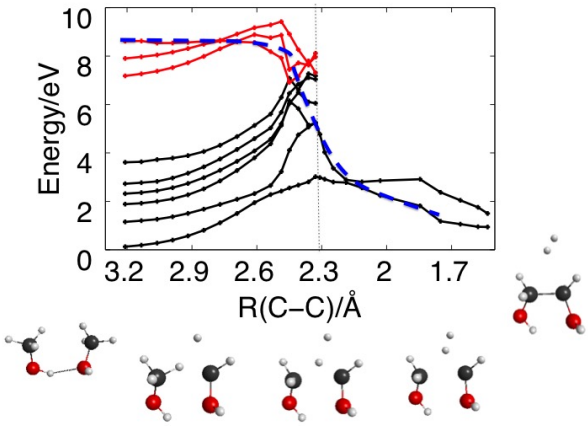

Fig. 6 Potential energy profiles associated with the anionic dimer along the minimum energy profile, calculated using CASPT2/cc-PVDZ. Shape resonances are shown in black while Feshbach resonances are shown in red. The blue dashed line indicates our proposed pathway towards reactivity. The vertical black dashed line indicates the position of the TS.

As evident from Fig. 6 all but the third Feshbach resonance are unreactive with respect to decreasing R(C-C) - all showing a gradual increase in PE *en-route* to the TS. In contrast, the third Feshbach resonance shows a gradual decline in PE, indicating facile reactivity with respect to decreasing R(C-C). At the local topography around the TS, the Feshbach and shape resonances have very similar energies and radiationless decay from the initially populated reactive Feshbach resonance to the lower energy resonances should be feasible. The gap between D_0 and D_1 however remains about 2 eV in both EOM and CASPT2 methods at the TS geometry. But beyond the TS, the remaining topography *en-route* to the products, returns an avoided crossing between D_0 and D_1 states, at R(C-C) = 2.2 Å. This likely indicates the presence of a conical intersection - motion through which is likely to lead to $D_0 \leftarrow D_1$ internal conversion. These topographic details are illustrated by the blue dashed curve in Fig. 6.

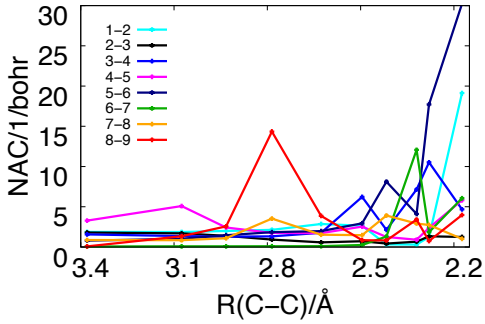

Fig. 7 Magnitude of the nonadiabatic coupling vector between pairs of states calculated at the CASSCF level.

In order to confirm that the proposed radiationless cascade can take place along the pathway we examine the nonadiabatic coupling. Fig. 7 shows the magnitude of the nonadiabatic coupling vector along the path for all pairs of adjacent states. The plot very clearly shows that there is strong coupling between the initially populated Feshbach resonance and the resonances below that. Around R(C-C)=2.8 Å the coupling between states 9 and 8 reaches a maximum (indicative of the conical intersection at that point) which should facilitate fast radiationless transition between these resonances. After that there are subsequent strong couplings which can eventually facilitate decay to the lowest resonance. This is physically explained by the fact that the Feshbach and shape resonances mix along the reaction pathway and their character is not as different anymore. Couplings between sequential resonances show that radiationless decay should be very fast all the way to the ground anionic state.

Finally, even though we have not calculated the lifetimes along the path, we can attempt some predictions based on how far energetically a resonance is from its parent neutral state. Fig. S6 in ESI† shows both the neutral and anion states at the EOM-EA-CCSD level and can be used to estimate the stability of resonances. The lifetime is initially long because the Feshbach resonance is close energetically to its parent triplet neutral state. This is typical of core-excited Feshbach resonances and is also in agreement with previous work on methanol monomer. The lifetime should be similar as long as the population is on a core-excited resonance. After nonadiabatic transitions to the shape resonances the parent neutral state becomes the singlet ground state. Since these transitions occur close to the transition state (based on the couplings) the shape resonances should again be more stable because the gap with the neutral state is small. At the transition state actually Fig. S6 shows that the first anionic state is stable since it has a positive electron affinity. After the transition state however the resonance becomes less stable again as the gap from the neutral state increases. At that point the electron can detach

easily.

Even though we have not calculated a minimum energy path, we believe the path shown here can be used to qualitatively show how the reaction can occur. The main features are that the initial long-lived Feshbach resonance is coupled to the shape resonances. Eventually the coupling will lead to the lowest resonance. If that happens before the transition state then one can assume that reactivity will not occur as the driving force will be stronger to go back to the initial reactants. If however the transition to the lowest resonance occurs after the transition state then the gradients suggest that the reaction can take place. Overall, even if some bifurcation occurs our work shows that at least some population should lead to the products.

4 General Discussion and Conclusions

With the topographic details of the PE profiles in Fig. 5 and 6 in mind, we now propose a plausible mechanism for the experimentally observed fragment products following low energy electron irradiation. An incident electron, with kinetic energies in the range 7-20 eV, may lead to a scattering or reactive event. The former leads to deflection of the incident electron whilst the latter would form an electron-attached state of the nascent anion. Provided an incident electron is sufficiently energetic, a scattering event is likely to form electronically excited neutral methanol molecules and follow an excited-state reaction path akin to those shown in Fig. 5. Instead, a reactive event may lead to an electron attached state of a methanol molecule and show energetics akin to the profiles in Fig. 6. In the present study we show that our paths contain a lower energy and more favorable topography when in an anion form, although it should be kept in mind that these are not minimum energy paths.

One caveat needs to be addressed here; the work by Boamah et al. shows the formation of neutral fragments - in which the authors propose neutral excited state chemistry followed by scattering of the incident low energy electron.[18] Given the incident electron kinetic energy range, we cannot rule this process out but we are also unable to rule out fragmentation via electron-attachment and evolution along an anionic excited-state reaction path. We hereby justify our reasoning for the latter mechanism which is schematically represented by the blue dashed curve in Fig. 6. The PE profiles reveal that electron-attachment at electron kinetic energies in excess of 7 eV may plausibly lead to electron attachment to the third Feshbach resonance (i.e. the third red PE profile in Fig. 6). Overall, the results from Figs. 6 and 7 indicate that the third Feshbach resonance diabatically correlates with the ground resonance states of the ethylene glycol + H_2 products, leading to the conclusion that that electron-attachment to this state may promote DEA-mediated products. Such an event may occur providing that the nuclear motions that drive the excited state chemistry along an anionic path are faster than electron detachment, which is usually the case for Feshbach resonances. Such processes would necessarily yield anion fragments which could then electron detach post-formation or as the nascent products form within the time-of-flight - ensuring that the ultimate detected products encompass a neutral fragment fingerprint. Neutral products may also be formed if the reaction process along the anionic path doesn't survive the reaction path, leading to electron-detachment. Since the neutral and anion ground states are close in energy and that the PE profile of the neutral path is reactive from the TS to the products, electron-detachment would ensure the formation and subsequent detection of neutral products. One may consider the electron catalyzing the reaction since it is not present at the products. Examples of electron catalyzed reactions have been discussed in the literature.[50,51] As a final remark on the neutral vs. anion chemistry, we note the study by Boyer et al.[19] who recently identified an abundance of CH_3O radicals in the temperature-programmed desorption data - concluding that the formation of ethylene glycol is likely prepared by electron-impact electronic excitation rather than DEA. Whilst this may be plausible at the high-energy limit of the electron-kinetic energy range we note that such radicals may indeed also arise via DEA in which the partner H carries the negative charge as H^- - forming $CH_3O + H^-$ asymptotic products - as shown by Slaughter and co-workers.[9] Notwithstanding, both electron-impact excitiation and DEA may be active in bulk methanol - in which the high kinetic energy regime is dominated by electron-impact excitation whilst the low kinetic energy regime is dominated by DEA.

We want to point out here that we were very careful to use a combination of theoretical approaches carefully tested and compared to experimental evidence in order to provide a basis for our conclusions for this mechanism. Theoretical approaches to treat resonances and DEA for molecules of the size studied here are still not well developed, so one has to be careful in their applicability. In this work, the Feshbach resonance, which is the initial step in the mechanism, is a well known long-lived resonance in methanol. It has been experimentally detected and there have been several previous theoretical calculations based on scattering which predict it has a long lifetime. We compare our results from the stabilization method to the previous theoretical and experimental results (see Table 2) and find a very good agreement for the position and less so for the lifetime. The agreement between the theoretical and the experimental resonance in methanol confirms that we use a reasonable approach. The remaining work on the dimer system does not use the stabilization method but small basis sets which avoid the continuum states.The comparison between the prediction from the stabilization method and experiment in methanol monomer (and the failure to be able to use it for the dimer) can be used as a benchmark for knowing the limits of stabilization methods and motivating further developments.

A final important note is that we recognize that our present dimeric system is a vast reduction in the dimensionality of an expected methanol ice crystal present on the surface of a comet. We also note that the expected low-entropy in a bulk ice crystal is likely to alter the excitation energies with respect to those obtained in the gas-phase. The lower disorder in a solid-state ice crystal is expected to enhance dipole-dipole interactions between neighboring methanol molecules. This is therefore expected to manifest in larger cross-sections for absorption to charge-transfer states. Notwithstanding, the present study is nonetheless very informative and serves to show the way in which a larger scale extrapolation of a simple dimeric system may form longer chain sugars on comets - which are routinely irradiated with secondary

low energy electrons with energies well within the 5-20 eV kinetic energy range. Such processes may have been important in driving the early planetary formations of prebiotic sugars. Given the inherent importance of such prebiotic reaction, we expect many more such studies in the future.

Conflicts of interest

There are no conflicts to declare.

Acknowledgements

The authors are grateful to Pratip Chakraborty for careful reading of our manuscript and to the National Science Foundation (grant number: CHE-1465138) for funding. MAF acknowledges Quaker Chemical Corporation for support.

Notes and references

1 J. Taillades, I. Beuzelin, L. Garrel, V. Tabacik, C. Bied and C. A, *Orig Life Evol Biosph*, 1998, **28**, 61–77.
2 A. Jalbout, *Orig Life Evol Biosph*, 2008, **38**, 489–497.
3 S. A. Sandford, P. P. Bera, T. J. Lee, C. K. Materese and M. Nuevo, *Top Curr Chem*, 2015, **356**, 123–164.
4 C. Walsh, R. A. Loomis, K. I. Oberg, M. Kama, M. L. R. van 't Hoff, T. J. Millar, Y. Aikawa, E. Herbst, S. L. Widicus Weaver and H. Nomura, *Astrophys. J. Lett.*, 2016, **823**, L10.
5 M. C. Boyer, N. Rivas, A. A. Tran, C. A. Verish and C. R. Arumainayagam, *Surface Science*, 2016, **652**, 26–32.
6 K. I. Oberg, *Chem. Rev.*, 2016, **116**, 9631–9663.
7 B. W. Carroll and D. A. Ostlie, *An Introduction to Modern Astrophysics*, Pearson, 2nd edn., 2007.
8 C. J. Bennett, C. Pirim and T. M. Orlando, *Chem. Rev.*, 2013, **113**, 9086–9150.
9 D. S. Slaughter, D. J. Haxton, H. Adaniya, T. Weber, T. N. Rescigno, C. W. McCurdy and A. Belkacem, *Phys. Rev. A*, 2013, **87**, 052711.
10 N. Brouillet, D. Despois, X.-H. Lu, A. Baudry, J. Cernicharo, D. Bockelée-Morvan, J. Crovisier and N. Biver, *Astron. Astrophys.*, 2015, **576**, A129.
11 B. A. McGuire, C. N. Shingledecker, E. R. Willis, A. M. Burkhardt, S. El-Abd, R. A. Motiyenko, C. L. Brogan, T. R. Hunter, L. Margulés, J.-C. Guillemin, R. T. Garrod, E. Herbst and A. J. Remijan, *Astrophys. J.*, 2017, **851**, L46.
12 D. Tuna, A. L. Sobolewski and W. Domcke, *Phys. Chem. Chem. Phys.*, 2014, **16**, 38–47.
13 S. Pizzarello, G. W. Cooper and G. J. Flynn, in *The Nature and Distribution of the Organic Material in Carbonaceous Chondrites and Interplanetary Dust Particles*, University of Arizona Press, 2006, pp. 625 –651.
14 I. I. Fabrikant, S. Eden, N. J. Mason and J. Fedor, *Advances in Atomic, Molecular, and Optical Physics*, 2017, **66**, 545–657 (and references therein).
15 J. Simons, *Adv. Quantum Chem.*, 2007, **52**, 171 (and references therein).
16 Y. Kawarai, T. Weber, Y. Azuma, C. Winstead, V. McKoy, A. Belkacem and D. S. Slaughter, *J. Phys. Chem. Lett.*, 2014, **5**, 3854.
17 M. A. Fennimore, T. N. V. Karsili and S. Matsika, *Phys. Chem. Chem. Phys.*, 2017, **19**, 17233–17241.
18 M. D. Boamah, K. K. Sullivan, K. E. Shulenberger, C. M. Soe, L. M. Jacob, F. C. Yhee, K. E. Atkinson, M. C. Boyer, D. R. Haines and C. R. Arumainayagam, *Faraday Discuss*, 2014, **168**, 249–266.
19 M. C. Boyer, M. D. Boamah, K. K. Sullivan, C. R. Arumainayagam, M. Bazin, A. D. Bass and L. Sanche, *J. Phys. Chem. C*, 2014, **118**, 22592–22600.
20 K. K. Sullivan, M. D. Boamah, K. E. Shulenberger, S. Chapman, K. E. Atkinson, M. C. Boyer and C. R. Arumainayagam, *MNRAS*, 2016, **460**, 664–672.
21 S. Esmaili, A. D. Bass, P. Cloutier, L. Sanche and M. A. Huels, *J. Chem. Phys.*, 2017, **147**, 224704.
22 Z. Chen, A. T. J. B. Eppink, B. Jiang, G. C. Groenenboom, X. Yang and D. H. Parker, *Phys. Chem. Chem. Phys.*, 2011, **13**, 2350–2355.
23 S. Harich, J. J. Lin, Y. T. Lee and X. Yang, *J. Phys. Chem. A*, 1999, **103**, 10324–10332.
24 J.-D. Chai and M. Head-Gordon, *Phys. Chem. Chem. Phys.*, 2008, **10**, 6615.
25 T. H. Dunning Jr., *J. Chem. Phys.*, 1989, **90**, 1007–1023.
26 C. Peng and H. B. Schlegel, *Israel J. Chem.*, 1993, **33**, 449–454.
27 A. I. Krylov, *Annu. Rev. Phys. Chem.*, 2008, **59**, 433.
28 K. Anderson, P. A. Malmqvist and B. O. Roos, *J. Chem. Phys.*, 1992, **96**, 1218.
29 J. Simons, *J. Chem. Phys.*, 1981, **75**, 2465.
30 J. S.-Y. Chao, M. F. Falcetta and K. D. Jordan, *J. Chem. Phys.*, 1990, **93**, 1125.
31 K. D. Jordan, V. K. Voora and J. Simons, *Theor. Chem. Acc.*, 2014, **133**, 1445.
32 K. D. Jordan, *Chem. Phys.*, 1975, **9**, 199.
33 K. D. Jordan, *J. Mol. Spectrosc.*, 1975, **56**, 329–331.
34 M. A. Fennimore and S. Matsika, *Phys. Chem. Chem. Phys.*, 2016, **18**, 30536–30545.
35 M. A. Fennimore and S. Matsika, *Phys. Chem. Chem. Phys.*, 2017, **19**, 29005.
36 M. J. Frisch, G. W. Trucks, H. B. Schlegel, G. E. Scuseria, M. A. Robb, J. R. Cheeseman, G. Scalmani, V. Barone, B. Mennucci, G. A. Petersson, H. Nakatsuji, M. Caricato, X. Li, H. P. Hratchian, A. F. Izmaylov, J. Bloino, G. Zheng, J. L. Sonnenberg, M. Hada, M. Ehara, K. Toyota, R. Fukuda, J. Hasegawa, M. Ishida, T. Nakajima, Y. Honda, O. Kitao, H. Nakai, T. Vreven, J. A. M. Jr., J. E. Peralta, F. Ogliaro, M. Bearpark, J. J. Heyd, E. Brothers, K. N. Kudin, V. N. Staroverov, R. Kobayashi, J. Normand, K. Raghavachari, A. Rendell, J. C. Burant, S. S. Iyengar, J. Tomasi, M. Cossi, N. Rega, J. M. Millam, M. Klene, J. E. Knox, J. B. Cross, V. Bakken, C. Adamo, J. Jaramillo, R. Gomperts, R. E. Stratmann, O. Yazyev, A. J. Austin, R. Cammi, C. Pomelli, J. W. Ochterski, R. L. Martin, K. Morokuma, V. G. Zakrzewski, G. A. Voth, P. Salvador, J. J. Dannenberg, S. Dapprich, A. D. Daniels, O. Farkas, J. B. Foresman, J. V. Ortiz, J. Cioslowski and D. J.

Fox, *Gaussian 09 Revision E.01, Gaussian Inc. Wallinford CT, 2009*.

37 H.-J. Werner, P. J. Knowles, G. Knizia, F. R. Manby and M. Schütz, *Wiley Interdiscip. Rev.: Comput. Mol. Sci.*, 2012, **2**, 242–253.

38 Y. Shao, L. Fusti-Molnar, Y. Jung, J. Kussmann, C. Ochsenfeld, S. T. Brown, A. T. B. Gilbert, L. V. Slipchenko, S. V. Levchenko, D. P. O'Neill, R. A. D. Jr., R. C. Lochan, T. Wang, G. J. O. Beran, N. A. Besley, J. M. Herbert, C. Y. Lin, T. V. Voorhis, S. H. Chien, A. Sodt, R. P. Steele, V. A. Rassolov, P. E. Maslen, P. P. Korambath, R. D. Adamson, B. Austin, J. Baker, E. F. C. Byrd, H. Daschel, R. J. Doerksen, A. Dreuw, B. D. Dunietz, A. D. Dutoi, T. R. Furlani, S. R. Gwaltney, A. Heyden, S. Hirata, C. Hsu, G. Kedziora, R. Z. Khaliullin, P. Klunzinger, A. M. Lee, M. S. Lee, W. Z. Liang, I. Lotan, N. Nair, B. Peters, E. I. Proynov, P. A. Pieniazek, Y. M. Rhee, J. Ritchie, E. Rosta, C. D. Sherrill, A. C. Simmonett, J. E. Subotnik, H. L. W. III, W. Zhang, A. T. Bell, A. K. Chakraborty, D. M. Chipman, F. J. Keil, A. Warshel, W. J. Hehre, H. F. S. III, J. Kong, A. I. Krylov, P. M. Gill and M. Head-Gordon, *Phys. Chem. Chem. Phys.*, 2006, **8**, 3172.

39 M. S. Gordon and M. W. Schmidt, in *Advances in electronic structure theory: GAMESS a decade later*, ed. C.E.Dykstra, G.Frenking, K.S.Kim and G.E.Scuseria, Elsevier, Amsterdam, 2005, pp. 1167–1189.

40 Y. Wen, J. Segall, M. Dulligan and C. Wittig, *J. Chem. Phys.*, 1994, **101**, 5665.

41 M. Lucas, Y. Liu, R. Bryant, J. Minor and J. Zhang, *Chem. Phys. Lett.*, 2015, **619**, 18–22.

42 B.-M. Cheng, M. Bahou, W.-C. Chen, C. hui Yui, Y.-P. Lee and L. C. Lee, *J. Chem. Phys.*, 2002, **117**, 1633.

43 K. Varela, L. R. Hargreaves, K. Ralphs, M. A. Khakoo, C. Winstead, V. McKoy, T. N. Rescigno and A. E. Orel, *J. Phys. B: At. Mol. Opt. Phys.*, 2015, **48**, 115208.

44 B. C. Ibenescu, O. May, A. Monney and M. Allan, *Phys. Chem. Chem. Phys.*, 2007, **9**, 3163.

45 D. Bouchiha, J. D. Gorfinkiel, L. G. Caron and L. Sanche, *J. Phys. B: At. Mol. Opt. Phys.*, 2007, **40**, 1259–1270.

46 V. S. Prabhudesai, A. H. Kelkar, D. Nandi and E. Krishnakumar, *Phys. Rev. Lett.*, 2005, **95**, 143202.

47 T. Skalický and M. Allan, *J. Phys. B: At. Mol. Opt. Phys.*, 2004, **37**, 4849.

48 J. A. Fournier, C. J. Johnson, C. T. Wolke, G. H. Weddle, A. B. Wolk and M. A. Johnson, *Science*, 2014, **344**, 1009–1012.

49 A. L. Sobolewski and W. Domcke, *J. Phys. Chem. A*, 2001, **105**, 9275–9283.

50 D. Davis, V. P. Vysotskiy, Y. Sajeev and L. S. Cederbaum, *Angew. Chem. Int. Ed.*, 2011, **50**, 4119 –4122.

51 D. Davis, V. P. Vysotskiy, Y. Sajeev and L. S. Cederbaum, *Angew. Chem. Int. Ed.*, 2012, **51**, 8003 –8007.